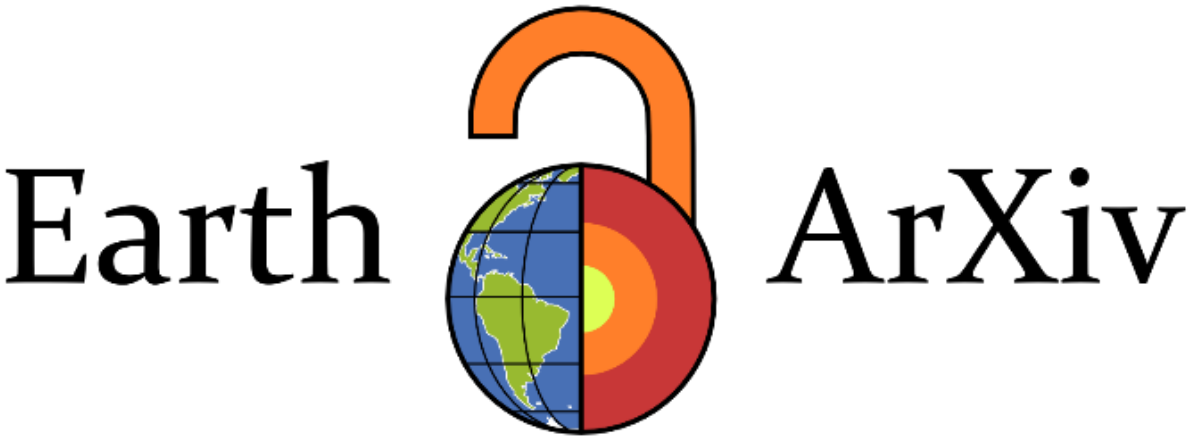

Interpretable Relations between Tropical Sea Surface Temperature and U.S. Precipitation in Winter Season Forecasts

Michelle L. L'Heureux,[a] Michael K. Tippett,[b]

[a] *NOAA/NWS/NCEP/Climate Prediction Center, College Park, MD*

[b] *Department of Applied Physics and Applied Mathematics, Columbia University, New York, NY*

Corresponding author: Michelle L. L'Heureux, michelle.lheureux@noaa.gov

ABSTRACT: We explore the large-scale relations between anomalies of global tropical sea surface temperature (SST) and U.S. precipitation to assess the sources of December–February (DJF) predictability and skill. Canonical Correlation Analysis (CCA) is applied to forecasts from NOAA's latest seasonal prediction system, the Seamless System for Prediction and EArth System Research (SPEAR). We find that DJF skill can largely be recreated using 2 SST principal components (PC) and 4 precipitation Principal Components (PCs). However, the leading CCA modes based on these PCs are a blend of two climate signals, El Niño-Southern Oscillation (ENSO) and linear trends, which makes them difficult to interpret. We separate the trend and ENSO signals using partial CCA whereby CCA is applied twice: once to data with linear trends removed and once to data with Niño-3.4 index linearly removed. After both signals are removed, CCA find no consequential relations. Therefore, ENSO and linear trends alone explain the predictable parts of the winter forecast of tropical SST and US precipitation anomalies. Despite SPEAR model predictions representing both linear and non-linear variability, skill is mostly explained by these simpler linear CCA patterns.

SIGNIFICANCE STATEMENT:

- Nearly all of the predictable signal in SPEAR can be reconstructed using only 2 SST and 4 precipitation principal components.
- Skillful December-February predictions of tropical sea surface temperature and U.S. precipitation are mostly driven by ENSO and linear trends.
- Partial canonical correlation analysis effectively untangles the physically distinct drivers of winter variability.

1. Introduction

Coupled climate prediction models are routinely run to support the real-time production of seasonal climate outlooks across many national meteorological and hydrological service agencies. These seasonal outlooks can prepare society and mitigate risks associated with impending shifts in temperature, precipitation, and other climatic variables. While the production of outlooks using prediction models is common, any single forecast is a combination of multiple factors and climate signals, and the exact breakdown of those factors is seldom obvious. Often a forecaster will compare an outlook to expected impacts from well-known drivers such as ENSO, but without a quantitative measure of, for instance, the ENSO contribution. Another complication arises when different drivers result in similar patterns that are easily confused with another. However, in real-time, crafting carefully designed, specialized model experiments to assess what is driving forecast accuracy, or skill, is often time and cost prohibitive, especially when there are forecast deadlines. Regardless, there are likely societal benefits from understanding the sources of seasonal prediction skill and being able to diagnose their contribution to a particular forecast.

Clarifying the drivers of the forecast is important for reasons that go beyond curiosity—it enhances transparency and fosters greater confidence in seasonal climate outlooks. In this study, we take a closer look at the features in DJF global tropical sea surface temperature anomalies that are responsible for DJF U.S. precipitation skill in NOAA's SPEAR model (Delworth et al. 2020). SPEAR is a periodic contributor to the real-time North American Multi-model ensemble (NMME), which is used in operational seasonal climate outlooks (Kirtman et al. 2014; Becker et al. 2022). Specifically, we have two aims: 1) to identify the drivers that result in skillful forecasts

on average, and 2) to explain what combination of drivers account for the structure and amplitude of the forecasted anomalies. These two objectives are not necessarily tied to each other because, hypothetically, the SPEAR model might predict variability that fails to contribute meaningfully to forecast skill.

One obstacle in understanding the wintertime relationships between tropical SST anomalies and U.S. precipitation is the high dimensionality of the datasets. To diagnose the association between two large time-varying geographic fields, dimension reduction of some kind is common. A popular technique in climate analysis is to first form univariate indices related to the possible source, such as ENSO, and then to correlate this index with other fields (e.g., precipitation anomalies). An index can be formed through a simple regional average (e.g., SST in the Niño-3.4 region) or through more advanced techniques like rotated or unrotated Principal Component (PC) Analysis. However, a drawback in this approach is that one must, a priori, select and identify the drivers of variability. Canonical correlation analysis (CCA) has the advantage of diagnosing the relationship between the global tropical oceans and U.S. precipitation anomalies while making relatively few assumptions.

In this study, CCA is chosen to find maximally correlated patterns between wintertime (DJF) anomalies of tropical SSTs and precipitation over the U.S. CCA finds the linear combinations that optimize the correlation between two time-varying, gridded (latitude-longitude) fields. The resulting canonical loading patterns are sorted into correlated pairs where each successive pair is constrained to be uncorrelated to the previous pairs. Because of its ability to search for strongly correlated patterns over large geographic domains, CCA is highly suitable to uncover the primary tropical SST drivers of precipitation variability. CCA has the added advantage of being mathematically interpretable, meaning there are unique closed-form solutions, and CCA-based predictions are the same as ones from PC regression (Tippett et al. 2008).

In recent years, a number of studies have examined the predictability of subseasonal-to-seasonal variability within SPEAR. "Predictability" is distinguished from "prediction skill," with the former often focused on how well a given model predicts itself (e.g., correlating predicted Niño-3.4 with predicted precipitation or one member against an ensemble mean), while the latter focuses on how well the model prediction compares to observations. Many studies that analyze SPEAR (Jia et al. 2023; Zhang et al. 2024; Clark et al. 2025) have used average predictability time (APT) analysis (DelSole and Tippett 2009a,b), which maximizes the lead-time integrated signal-to-total variance

ratio. While the subject of each study is distinct, APT analysis is applied to a single variable, and then relations with other variables are diagnosed by regressing or correlating the APT variate from one variable to a field of a different variable. So, while APT seeks to maximize the predictability of a single variable, CCA instead focuses on relationships between variables. Similarly, other studies (e.g. Chen et al. 2024) have examined sources of NMME skill by identifying the leading PCs of two variables, separately, and then regressing them onto corresponding fields. A limitation of this strategy is that it maximizes the covariance of each field independently instead of their mutual correlation.

By applying CCA to model data we can assess the model's predictability and then check if they are also the drivers of prediction skill. The relative importance of the leading CCA patterns can be examined by reconstructing the predictions using those patterns and evaluating how well they correlate to the observations (prediction skill) or to the model itself (predictability). If the reconstruction using only a few CCA patterns is sufficient to reproduce the model's prediction skill of U.S. winter precipitation, then it indicates that these patterns contain variability that is responsible for most of the skill while the remaining, higher-order modes constitute unpredictable noise. Knowledge of which features are essential to the model's skill can steer future model development. For instance, if the model's representation of snow cover or soil moisture is believed to be critical in certain seasons then it should be shown that they can meaningfully contribute to the model's predictability (e.g. Riddle et al. 2013). A lack of prediction skill does not necessarily mean that sources of predictability do not exist.

Section 2 describes the data and methods, Section 3 will cover the results, and Section 4 will summarize the primary findings and provide ideas for future investigation.

2. Data

Predicted SST and precipitation data from SPEAR were downloaded from the International Research Institute (IRI) for Climate and Society library, which offers monthly forecasts beginning in 1991, out to 12 months of lead time, with 15 members. For the real-time period beginning in early 2021, an extra 15 members are provided, but are not used to be consistent with the hindcast period. In this study, 34 December–February (DJF) seasons are considered (1991–92 to 2024–25), which matches the available SPEAR data. For seasonally averaged data, forecasts go out to 10

leads (starts are March–December), which means pooling the full model ensemble constitutes a 150-fold increase in samples over the observational record (34 x 15 x 10).

Monthly anomalies of SST and precipitation are computed by subtracting the lead-dependent monthly mean over the entire record. The monthly anomalies are then averaged into DJF seasonal means. The CPC Unified gauge-based gridded precipitation dataset (Chen et al. 2008) is used to compare against the leading CCA patterns from SPEAR. Observed SST anomalies come from NOAA OISSTv2.1 daily data (Huang et al. 2021).

3. Methods

Supplementary Figure 1 provides a conceptual flow chart to compute CCA using two time-varying fields of tropical sea surface temperature and U.S. precipitation anomalies. Because PCs are normalized, the final singular value decomposition (SVD) is applied to a matrix that is proportional to correlations. The method was invented by Hotelling (1936), and details to calculate CCA are provided in DelSole and Tippett (2022), among many others. CCA has been applied to diagnostics of geopotential height anomalies (Wallace et al. 1992), predictions of ENSO (Barnston and Ropelewski 1992), prediction of surface air temperature (Barnett and Preisendorfer 1987; Barnston and Smith 1996; Mo 2003), and precipitation predictions (Barnston and Smith 1996; Mo and Thiaw 2002; Rana et al. 2018; Wang et al. 2021). Fewer studies have applied CCA to exclusively model data to diagnose sources of predictability within a model (Pegion et al. 2026; Buchmann and DelSole in review). CCA is commonly applied to model data as a post-processing step. For large datasets with more features than samples, the dimensionality of the data needs to be reduced prior to the CCA to ensure that the covariance matrices used in CCA are invertible. To do this, studies often use PC analysis and apply a subjective cutoff to retain a certain amount of the original variance, such as 70-90% (e.g. Bretherton et al. 1992). However, as suggested by the downscaling example in (Tippett et al. 2008), in some cases less variance needs to be retained, and a few PCs are adequate.

CCA will invariably extract paired modes that optimize correlation for the given datasets, including cases which the apparent relationships arise from noise or sampling variability. We therefore prefer to identify meaningful, statistically significant patterns. Two methods are applied: (1) Mutual Information Criterion (MIC) to select the optimal PC truncation and a (2) Monte Carlo

re-sampling test to test whether the leading mode correlations are distinct from random noise. The MIC was applied to CCA by DelSole and Tippett (2021) and is designed to identify the number of PCs needed from each input field that minimizes the MIC. MIC strikes a balance between the maximizing mutual information captured by the retained PCs while minimizing the number of estimated parameters. We use observational data to select the number of PCs (Supp. Fig. 2, top panel), settling on 2 SST modes and 4 US precipitation modes. The MIC was also applied to each of the 15 members in SPEAR (Supp. Fig. 2, bottom panel), and the same 2/4 combo is found to be equal to a plurality of members (25%). While MIC identifies the PCA truncation, an additional test is needed to evaluate whether the leading canonical correlation is distinguishable from random sampling. To do this, a Monte Carlo re-sampling procedure is applied to observations and model data. If the calculated canonical correlations of the leading CCA mode exceeds 95% of the randomized correlations, then there is a statistically significant relationship between the precipitation and SST modes, and the null hypothesis of no relation is rejected. In the model data, there are correlations across members because of initialization, which means exceeding the correlations of random data is easier. To keep the original member correlations intact, we scramble the model data by target time.

In many climate applications, leading CCA modes can mix physically distinct signals when both contribute to covariability (e.g., ENSO variability and secular trends). To gain confidence that CCA is extracting meaningfully physical modes, "partial CCA" is also employed and is analogous to partial correlation. Partial CCA is a generalization of CCA in which the linear relationships between two multivariate sets of variables are evaluated after removing the influence of one or more control variables. Here, the control variables are ENSO and the linear trend. An "ENSO-focused" CCA pattern is acquired after subtracting a least-squares fit linear trend from the input data. A "Trend-focused" CCA pattern is obtained after linearly removing the Niño-3.4 index. Because each analysis is conducted on residual data, the extracted modes are separated with respect to the specified control by construction.

Data are also "reconstructed" meaning that the associated regression maps onto SST or precipitation anomalies are then weighted by their respective standardized index values. These reconstructions provide the basis for evaluating how much of the raw model skill is reproduced by using a truncated number of CCA modes. Further, the reconstructed predictions based on the

identified physical drivers (e.g., ENSO and trend) are correlated with the observations to assess the skill of these particular drivers. In addition, to understand the predictability within SPEAR, or which drivers help explain the predictions, the reconstructed forecasts are directly correlated against the raw, unaltered model predictions.

4. Results

a. Identifying the leading CCA patterns

Fig. 1 displays the leading two CCA modes computed using the observational data with 2 SST PCs and 4 precipitation PCs. The number of CCA modes is equal to the minimum number of input PCs. The top left panels show the timeseries of the canonical variates for CCA-1 (top row) and CCA-2 (second row). The Monte Carlo test shows that the leading CCA is statistically significant, with canonical correlations well in excess of the coefficients obtained from randomly re-sampling the data (bottom middle). For the leading CCA-1, the correlation between the SST and precipitation time series is quite high (r = 0.82) and the associated SST and precipitation anomaly regression maps (right panels) closely resemble those associated with ENSO, which dominates wintertime U.S. precipitation variability. Positive SST anomalies are evident in the central and eastern equatorial Pacific, with negative anomalies structured in a familiar horseshoe shape emanating from the western Pacific warm pool. Over the contiguous U.S., positive index values are linked to above-average precipitation over the southern tier of states, with below-average precipitation over parts of the northwestern US and Ohio and Tennessee valleys. The second leading CCA-2 time series is less well correlated (r=0.41), and both time series demonstrate a distinctive positive trend over time. The associated SST anomalies are positive over most of the tropical oceans, except for negative anomalies in the southeastern tropical Pacific. Over the United States, positive index values are associated with below-average precipitation extending from Texas to California and above-average precipitation centered over the southeast and Pacific Northwest.

While the CCA-1 and CCA-2 time series are constrained to be uncorrelated, there is similarity between CCA-1 and CCA-2, especially with regards to the SST time series (blue lines) with both having peaks coincident with strong El Niño events (1997–98, 2015–16, and 2023–24). The Niño-3.4 index is correlated to SST CCA-1 at r=0.92 and SST CCA-2 at r=0.36. The SST patterns associated with CCA-1 and CCA-2 also share similar SST anomalies in the eastern equatorial

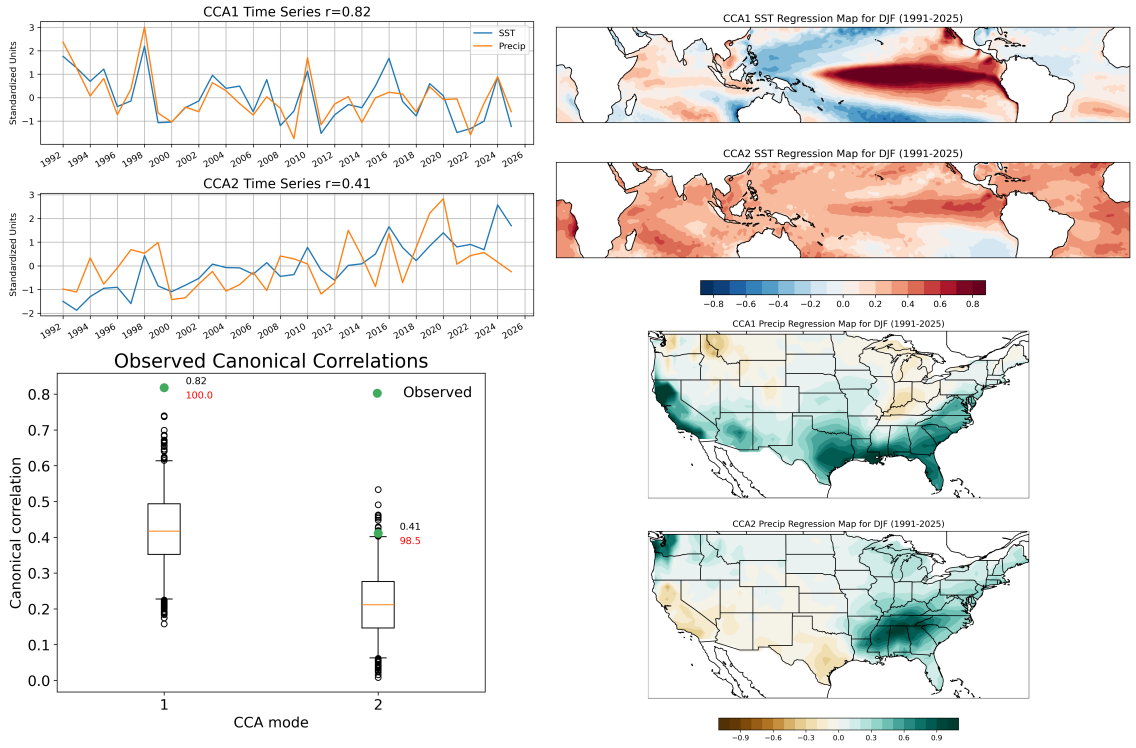

FIG. 1. In observations, the leading two CCA modes between anomalous US precipitation and tropical sea surface temperatures during DJF from 1991-92 to 2024-25. Standardized time series are shown in the upper left panels alongside their canonical correlations. SST and precipitation anomalies are regressed onto the leading time series and presented in the upper right and lower right panels (units in degree Celsius and mm/day per standardized index value) . Monte Carlo simulated canonical correlations for the leading two modes are shown in the bottom left panel. The observed percentiles within the simulated distributions are provided in red text and the canonical correlations are provided in black text. Data are based on OISSTv2.1and CPC Unified guage-based precpitation.

Pacific. Similarities between CCA-1 and CCA-2 are not limited to ENSO, with both time series showing trends, upward for CCA-1 and downward for CCA-2. Therefore, in observations, there is a mixture of ENSO variability and trends spread across the two leading CCA modes, which complicates their physical interpretation.

The same PCA truncation (2 SST and 4 precipitation PCs) was used to compute the CCA in SPEAR forecasts and is presented in Fig. 2. All forecast lead times and members are pooled together, which increases the sample size. In SPEAR, the CCA-1 time series resembles that of CCA-1 in observations (the correlation between observation and SPEAR CCA timeseries is r=0.79

for SST and r=0.53 for precipitation), with variability strongly linked to SPEAR's Niño-3.4 index (the correlation of SPEAR's Niño-3.4 index with SST CCA-1 is r=0.90 and precipitation CCA-1 is r=0.67). A slightly negative trend in the CCA-1 time series is also present.

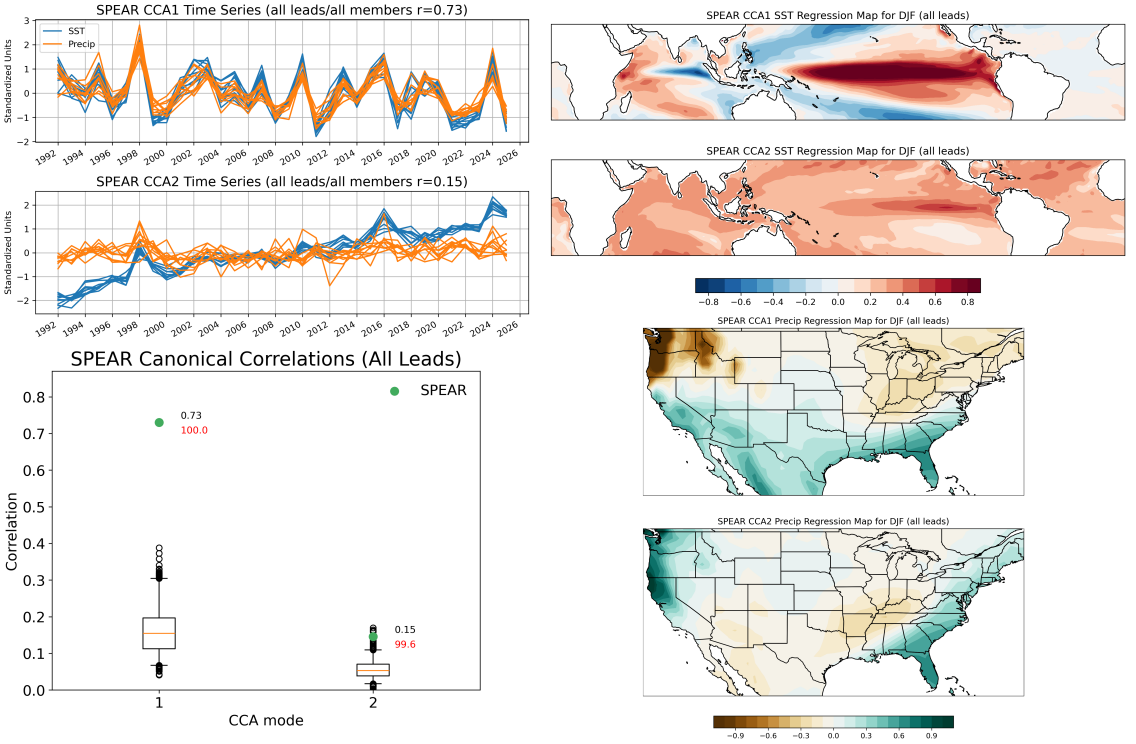

FIG. 2. As in Fig. 1 except displaying SPEAR ensemble means across all forecast leads for DJF targets. Each line in the top left panels is a different forecast lead time. Canonical correlations are based on pooling all forecast leads and members. Regression maps in the right panels are based on ensemble means pooled across all lead times.

For CCA-2, the SPEAR results diverge more substantially from the observations, and the canonical correlation is smaller in SPEAR (r=0.15). While the CCA-2 SST time series has a positive trend and similar variability with CCA-2 SST in observations (r=0.92), SPEAR's CCA-2 precipitation time series has almost zero correlation with CCA-2 precipitation in observations (r=.09) and a neutral trend and positive spike in 1997–98 for most lead times. SPEAR's SST CCA-2 association with SPEAR's Niño-3.4 is weaker (r=0.39), but similar to the correlation found in observations (r=0.36). The CCA-2 regression patterns are distinctive from observations, with more widespread positive trends and the disappearance of negative SST anomalies in the central and southeastern tropical Pacific in SPEAR. In precipitation, the minima in below-average precipitation shifts from

California/Texas in observations to the Tennessee valley in SPEAR. CCA-2 in SPEAR is also associated with above-average precipitation over the west and east coasts of the U.S. Overall, the biggest difference in CCA between SPEAR and observations stems from the U.S. precipitation component, with its notably lower correlations, especially in CCA-2 which has no trend in SPEAR. Aspects of Niño-3.4 and trends continue to be commingled among both CCA-1 and CCA-2 in observations and SPEAR.

SPEAR has the advantage of a larger sample size, which can result in significant leading modes despite small canonical correlations. While this provides some advantages, they may be partially offset by model biases and errors. Previous research has shown that seasonal forecast models have a positive trend bias in tropical Pacific SST anomalies that amplifies with forecast lead time (Shin and Huang 2019; L'Heureux et al. 2022; Beverley et al. 2024; Tippett and Becker 2024; Mayer et al. 2025; Patterson et al. 2025). Fig. 3 demonstrates that SPEAR is not an exception. The top row displays the observed linear tends in SST anomalies (left column) and precipitation anomalies (right column), with the first forecast lead time shown in the middle row and last forecast lead time in the bottom row. Because it is closest to the initial condition, the first lead in SPEAR closely resembles the observed trends, with negative SST trends extending from the southeastern tropical Pacific to the central Pacific, and a drying trend extending from California to Texas and over Florida. By lead-10, the negative trend in the southeastern tropical Pacific vanishes and positive trends dominate over most of the equatorial tropical Pacific. For precipitation, the overall SPEAR pattern remains similar to the first lead, but the trends are notably weak across the United States. At long forecast leads, it appears the shift toward the El Niño-like trend pattern in Pacific SSTs leads to a more muted La Niña-like pattern in precipitation that is seen in the first lead and observations.

Though CCA-2 is trend-like in both SPEAR (Fig. 2) and observations (Fig. 1), there are some clear differences between the two. As hinted in Fig. 3, it seems reasonable that the CCA of SPEAR better resemble the observations if only the first forecast lead time was analyzed. Fig. 4 shows the same CCA calculation as in Fig. 2 except considering only the first lead time in SPEAR. While the CCA-1 time series and patterns largely remain the same, there is a significant change in CCA-2. The canonical correlations increase from r=0.15 to r=0.30 and the precipitation time series no longer has a positive spike during 1997-98 as was the case for the pooled forecast leads presented in Fig. 2. A trend toward cooler SSTs in the southeastern tropical Pacific also becomes

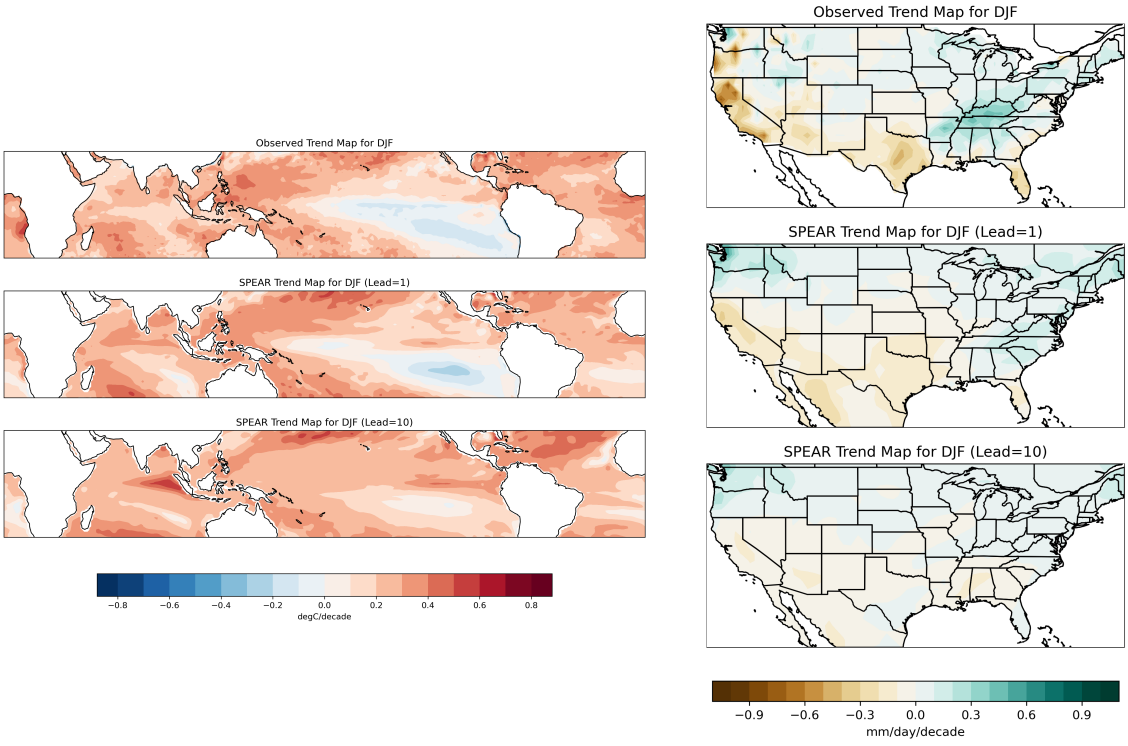

FIG. 3. Least-squares fit linear trend across DJF seasons from 1991-92 to 2024-25 for sea surface temperature anomalies (left panels) and US precipitation anomalies (right panels). The top row displays the observations, the middle row only shows the first forecast lead (L=1), and the bottom row shows the final forecast lead (L=10). Units are in degrees Celsius per decade and mm/day per decade.

more prominent when considering the first forecast lead, mimicking the observations. And, finally, a trend toward drier conditions over California and the Southwest returns when the first forecast lead is considered, better matching observations. In CCA-2, the only clear difference between first lead SPEAR and the observations is the opposite sign in precipitation over the southeastern U.S. Other than this discrepancy, the first lead using SPEAR better reflects observed trends, and so, for the remainder of this study, we will focus on analysis using this lead time.

To this point, we have justified using 2 SST PCs and 4 precipitation PCs on the basis that the MIC test identifies this as an optimal combination in both observations and among the SPEAR ensemble. However, there are two additional reasons this PC truncation is attractive. The left column of Fig. 5 shows the percent of variance explained by retaining the leading PCs of tropical SST (top panel) and U.S. precipitation (bottom panel) for the first-lead SPEAR forecasts during

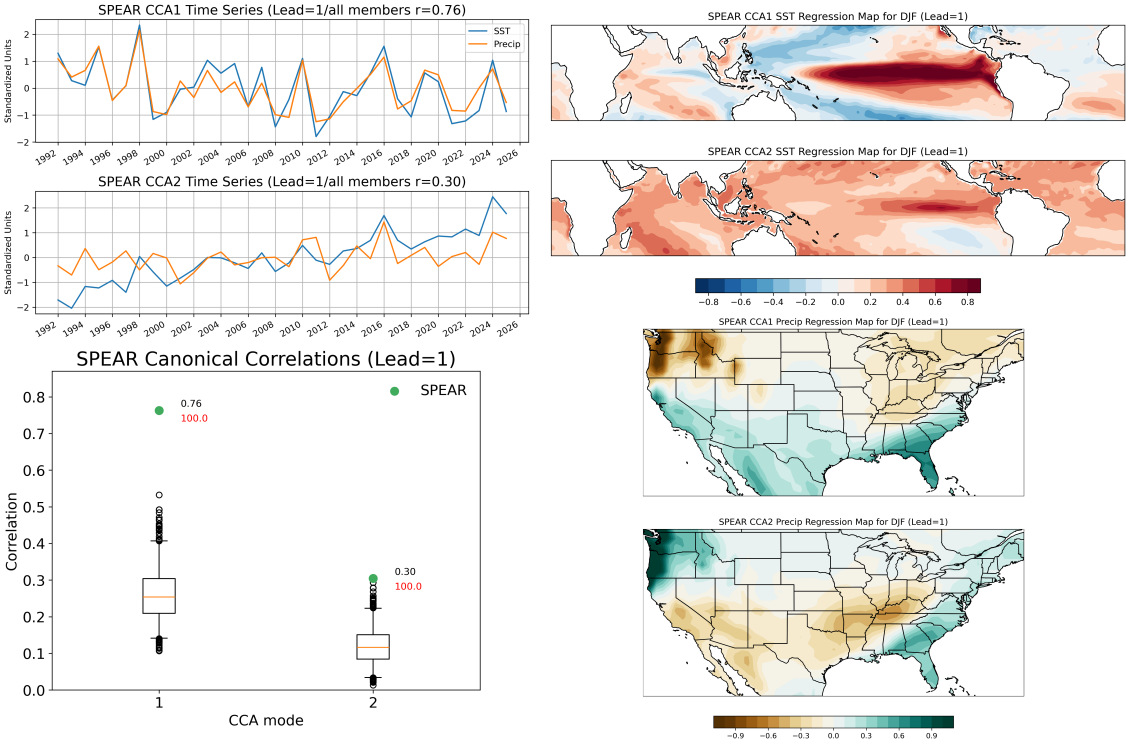

FIG. 4. As in Fig. 2 except displaying SPEAR ensemble means for a single forecast lead time (Lead=1).

DJF. Despite not being part of the selection criteria, it is this same combination that first explains at least 50% of the original data variance (52% of the SST variance and 55% of the precipitation variance).

Additionally, the right column of Fig. 5 shows the median forecast skill of the reconstructed SPEAR data as a function of the number of modes retained (the horizontal dashed line shows the model skill which remains higher for the first forecast lead, likely due to the contributions from the model's initial conditions). Tropical SST (top panel) nearly saturates in skill after 2 PCs are reconstructed, and U.S. precipitation nearly plateaus in skill after 4 PCs are reconstructed. While additional modes provide incremental increases in skill, DJF skill can largely be recreated using 2 SST PCs and 4 precipitation PCs.

Fig. 6 displays the first lead skill at each grid point for tropical SST anomalies (left panels) and U.S. precipitation anomalies (right panels). The skill of the raw SPEAR model predictions (top panels) is presented next to the skill of the reconstructed model data using the optimal combination of CCA (equivalently, the truncated PCs could also be used to compute the reconstruction). The

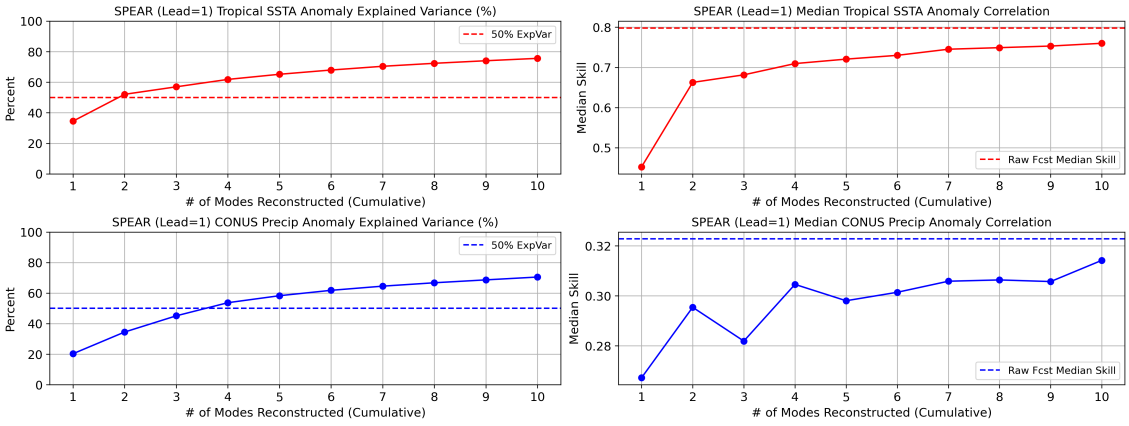

FIG. 5. First forecast lead SPEAR explained variance (in %; left panels) and median anomaly correlation (right panels) as a function of the number of PC modes reconstructed (cumulative). The top row is based on tropical SST anomalies and bottom row is for US precipitation anomalies (for the latitutde-longitude domains shown in Fig. 4). The dashed line in the left panels denotes 50% explained variance and the dashed line in the right panels is the median forecast correlation from the raw SPEAR model forecast for lead=1.

difference in skill between the reconstructed model patterns and raw model forecast is presented in the bottom panels.

Impressively, despite using only a few PCs in reconstruction, the raw model's skill appears to be a close match to the skill provided by its much reduced, reconstructed data. For U.S. precipitation, there are some differences but they are largely statistically insignificant. Along the global equator, the SST reconstruction mostly matches the skill of the model, especially over the central and eastern equatorial Pacific Ocean and the Indian Ocean. Statistically significant differences arise primarily in the off-equatorial regions (dots indicate significance at the 5% level), such as the northeast and southeast tropical Pacific, where model skill exceeds the reconstructed skill. Overall, the strong similarity between the raw model skill and the reconstructed model skill implies that the vast majority of SPEAR skill comes from two of the leading SST and precipitation CCA modes. The similarity between the skill of first-lead forecasts and the reconstruction is also impressive because the model has additional skill coming from the initial conditions that influences the early part of the month.

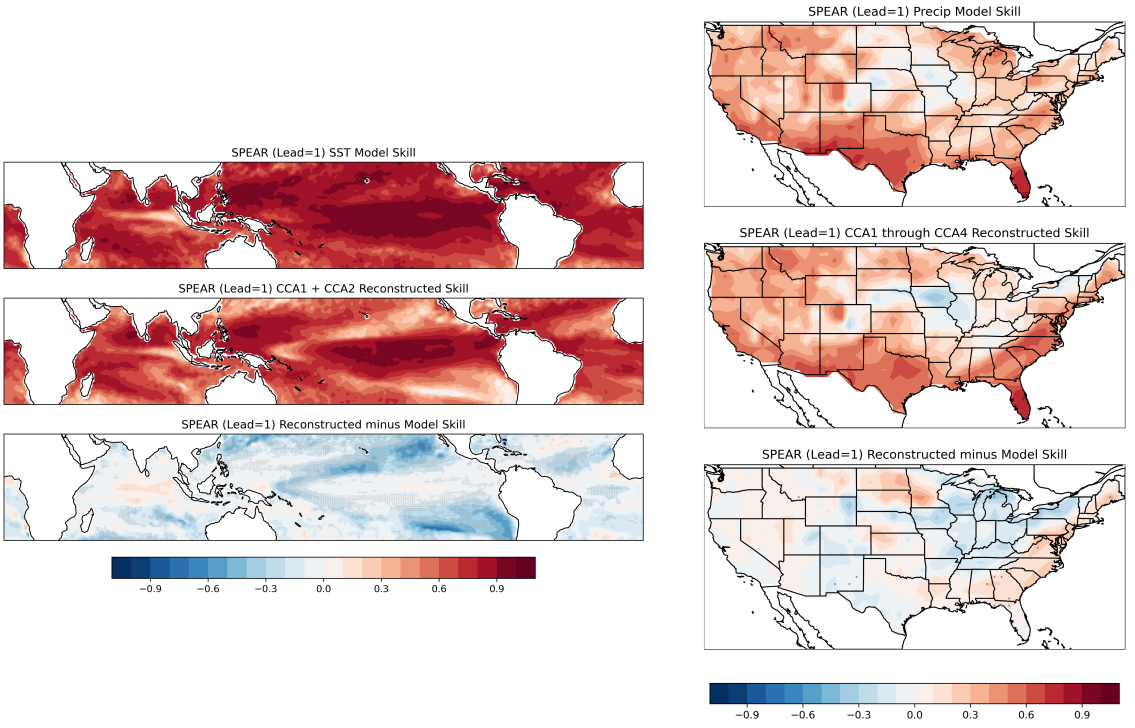

FIG. 6. First lead SPEAR forecast skill (anomaly correlations between model and observations) for the raw model forecast (top row), the reconstructions based on the leading CCA modes (middle row), and the difference between the middle and top rows (bottom row). Dots show where there are significant differences (passing the 5% level) in the squared residuals based on a 2-sided Wilcoxon signed-rank test. The left panels show skill for tropical SST anomalies and the right panels show skill for US precipitation anomalies.

b. Identifying Physically Interpretable CCA patterns

While CCA is mathematically interpretable, in the sense that its solutions have closed-form representations and those solutions have guaranteed optimality and orthogonality properties, their modes need not be physically interpretable, or associated with recognizable, known climate variability. The CCA method simply finds linear combinations of that data that maximizes correlations. In doing so, CCA mixes ENSO variability and trends. To separate ENSO variability and linear trends, we employ partial CCA by first linearly removing the Niño-3.4 index, and then, as a separate calculation, removing linear trends (Fig. 7). Separating the components enables forecast attribution, or asking "What part of the forecast is Niño-3.4 or linear trend related?" Later, we will use this CCA decomposition to provide a forecast attribution of the most recent DJF 2024–25 winter.

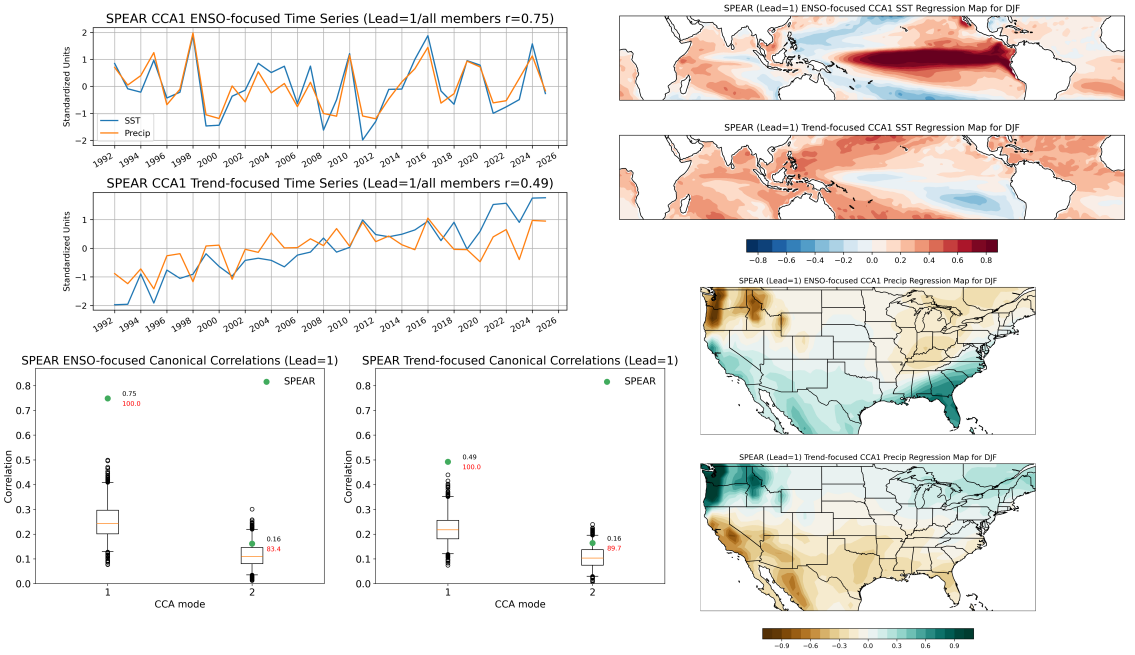

321 FIG. 7. As in Fig. 4, except showing the leading CCA1 time series and regression patterns associated with
322 ENSO-focused and Trend-focused partial CCAs.

323 Fig. 7 ("Trend-focused" panels) shows that, after removing Niño-3.4, the leading CCA-1 pattern
324 in the SPEAR first lead forecast reflects a clear positive trend with the canonical correlation between
325 the SST and precipitation timeseries (r=0.49) exceeding the correlations of the mixed trend mode
326 identified using the observations and SPEAR (Figures 1 and 4). The associated SST pattern with
327 CCA-1 not only shows a trend toward more negative SSTs in the southeastern Pacific as identified
328 previously, but the negative SSTs also emerge on the equator in the central Pacific Ocean. This
329 pattern more clearly reflects the 34-year wintertime SST trend in the observations (Figure 3). Over
330 the United States, the CCA-1 trend-focused mode is related to drier conditions over the southern
331 tier of states, and wetter conditions across the northwestern and northeastern states. The Monte
332 Carlo test shows that the first mode passes the 5% level of statistical significance and so we can
333 reject the null hypothesis that the time series are independent. The second mode is not significant
334 either (DelSole and Tippett 2022), and this result is consistent with an MIC analysis that suggests
335 only 1 mode is left after Niño-3.4 is regressed out (not shown).

336 Fig. 7 ("ENSO-focused" panels) displays the first lead SPEAR CCA after subtracting the linear
337 trend. Here, conventional ENSO variability emerges in the leading CCA-1 time series and SST

and precipitation anomalies (the canonical correlation is r=0.75). SPEAR's correlations between Niño-3.4 and CCA-1 also increases compared to the lead-1 SPEAR results without linear removal (r=0.96 for ENSO-focused SST CCA-1 vs. r = 0.88 for no removal SST CCA-1). As expected, this method eliminates the slight negative trend that was evident in the SPEAR and observational data (Figures 1 and 4). Based on the Monte Carlo, CCA-1 is also statistically significant.

These results demonstrate that the linear removal of Niño-3.4 and the trend effectively untangle the physical drivers of winter variability, which are commingled among the original CCA-1 and CCA-2 data. Further, the linear removals also result in secondary modes that are both statistically and physically insignificant, thereby conveniently identifying a single mode associated with ENSO and linear trend signals in SPEAR forecasts.

Presumably, if SPEAR forecasts only contain two meaningfully physical patterns, an ENSO and trend pattern, then the simultaneous removal of both should result in statistically insignificant patterns and lack of forecast skill. Fig. 8 shows the CCA patterns that remain after this calculation. While the SST timeseries and patterns associated with the leading CCAs has some similarity to the patterns after the respective linear removals (Fig. 7), neither CCA-1 or CCA-2 are statistically significant at the 5% level after the simultaneous removal. The canonical correlations are considerably smaller as well (r=0.30 and r=0.16), with the SST and precipitation time series explaining less than 10% of the variance.

The top two rows of Fig. 9 display the SPEAR model skill next to the reconstructed skill of the original CCA shown in Fig. 4. After the simultaneous linear removal of Niño-3.4 and the trend (Fig. 8), the resulting skill of the reconstruction based on the leading 2 SST PCs and 4 precipitation PCs is presented in the third row of Fig. 9. For SST (left panels), the ENSO/trend-removed reconstruction has positive skill in areas roughly orthogonal to the original CCA data reconstruction. This is not the case for U.S. precipitation (right panels), and the reconstruction, even after the linear removal of Niño-3.4 and trends, has some skill in roughly the same areas as the CCA reconstruction based on original data. For U.S. precipitation, one reason for the spatial overlap in skill may be that the leftover patterns, despite not being statistically significant, can overfit the data in the same regions that are influenced by ENSO and linear trends. Tropical SST has less exposure to this same overfitting because the residual leading patterns cover a broader

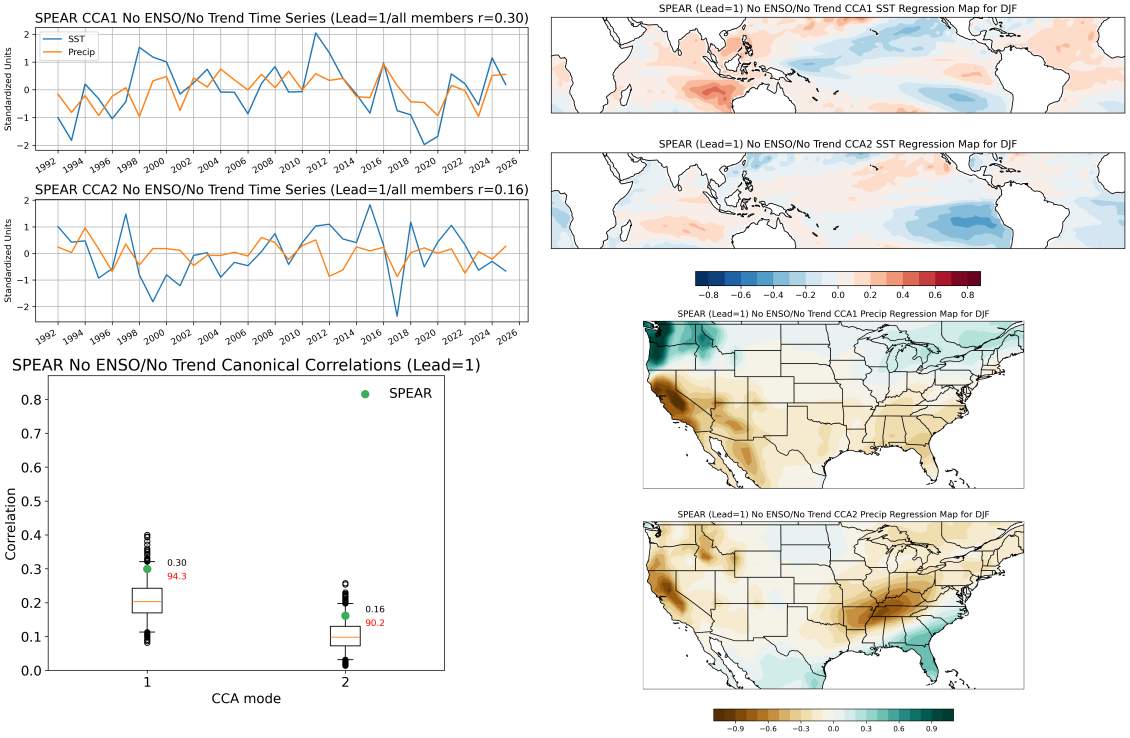

FIG. 8. As in Fig. 4, except showing the leading two CCA time series and regression patterns after linearly removing both Niño-3.4 and the linear trend.

geographic domain than U.S. and contain less overlap with the regions influenced by ENSO and the trend.

Apparent overfitting aside, the bottom panel of Fig. 9 (which subtracts the second row from the third row) demonstrates that the reconstructed skill is significantly reduced after the removal of Niño-3.4 and the linear trend. The loss in skill is particularly acute for tropical SSTs, with widespread statistically significant losses in skill over the domain. The apparent gains in skill associated with the removal of Niño-3.4 and trends are largely insignificant, with a few local exceptions. For precipitation, the change in skill is not as pronounced as for SST, but there are statistically significant decreases in skill over the southern tier of the US and the mid-Atlantic. Small regions with an increase in skill are generally not significant.

In making seasonal predictions, operational forecasters occasionally use SPEAR model output, as part of the NMME. A common question is what factors are driving the seasonal prediction, which is often unclear unless targeted experiments are performed with coupled ocean-atmosphere GCM, which is an expensive undertaking that is difficult to do in real time. While the leading two CCA

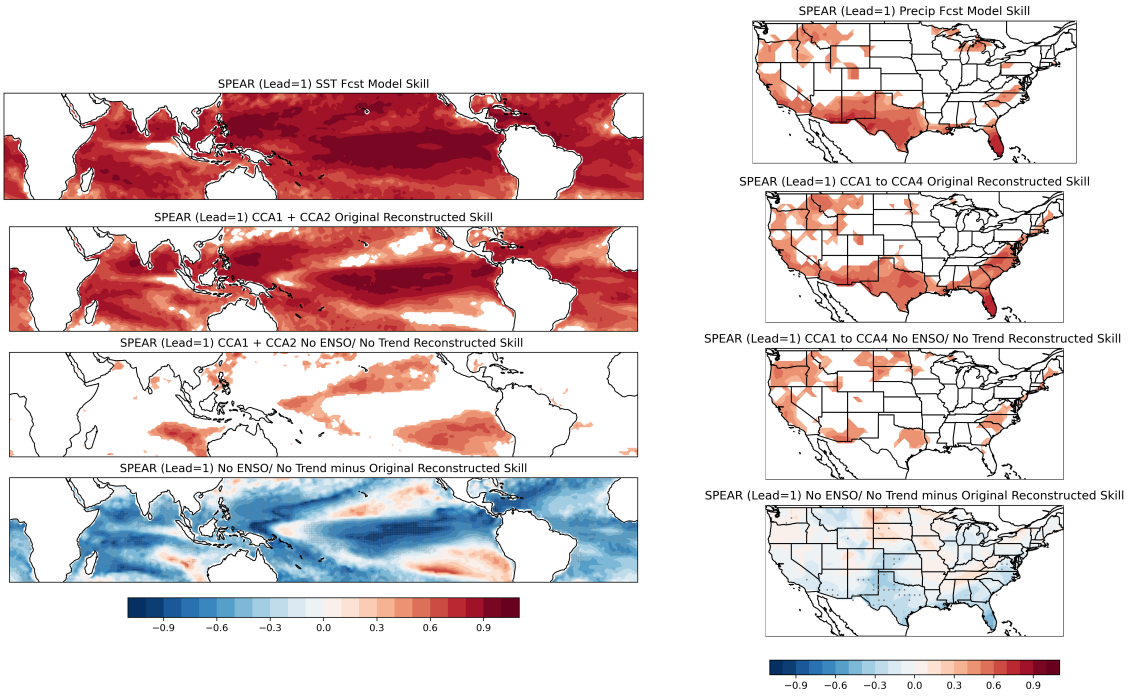

FIG. 9. The first two rows of Fig. 6 are reproduced in the top two rows, except now displaying only regions with forecast skill that pass the 5% level based on a t-test for the Pearson's correlation coefficient. The third row follows the same convention and shows the forecast skill for the reconstructions after linearly removing Niño-3.4 and the trend. The bottom row displays the difference between the third row and the second row (dots show where there are significant differences (passing the 5% level) in the squared residuals based on a 2-sided Wilcoxon signed-rank test). The left panels show skill for tropical SST anomalies and the right panels show skill for US precipitation anomalies

modes of SPEAR and observational data represent some unspecified blend of ENSO and trends, the advantage of partial CCA is to show there are largely two distinct, physically interpretable patterns. Successive CCA patterns are insignificant and do not provide additional sources of prediction skill. To leverage the ENSO-focused and trend-focused patterns and to aid forecasters in making forecast attributions, multiple linear regression (MLR) is used to quantify each component's relations with the first lead SPEAR predictions. MLR is used because the leading predictors do not derive from a single CCA calculation and therefore exhibit some correlation. We confirm that skill from MLR is indistinguishable from the skill using original leading CCA patterns, and that this level of skill is also equivalent to the skill of the raw SPEAR predictions (Supp. Fig. 3).

How much of the SPEAR forecasts are associated with the model's reconstruction of ENSO and trend? Fig. 10 displays the correlation between the reconstructions of SST (left panels) and US precipitation (right panels) and the lead=1 SPEAR forecasts. As shown in the second row, the model's combined (ENSO and Trend) reconstruction is significantly correlated over large areas of the model's forecast of U.S. precipitation and tropical SST anomalies. Impressively, even though the SPEAR forecast is initialized with ocean–land–cryosphere–atmosphere anomalies across the globe, which provide possible sources of winter skill, the leading modes of just tropical SST and U.S. precipitation are able to account for a high amount of the variability in the prediction. Digging deeper, it appears the bulk of the correlations is largely attributable to ENSO in the equatorial Pacific and over the U.S. However, linear trends dominate the SPEAR forecast in many of the other oceans and outside of the equatorial Pacific. In the U.S., linear trends appear to account for most of the model forecasts in the southwestern and south-central U.S. Over the southeast, linear trends are slightly anti-correlated, implying that the trends slightly oppose the model's forecasts. In contrast, for ENSO, some of the strongest correlations in the U.S. are found in the southeastern U.S.

In the end, the SPEAR forecast can be recreated using only 2 CCA patterns corresponding to ENSO and the Trend, which are presented in Fig. 7. Especially for US precipitation, the correlations with the combined (ENSO + Trend) reconstructed patterns are higher than the model's own skill (compare first row with second row). This is possible because the forecast is driven by predictable signals (predictability), whereas the model's prediction skill depends on observations and will be influenced, to some degree, by noise and sampling. Compared to U.S. precipitation, tropical SSTs are inherently more predictable based on the closer correspondence between the reconstruction correlations and model skill.

Fig. 11 illustrates a forecast attribution based on the DJF 2024–25 winter which was characterized by borderline La Niña conditions. The indices presented in the top row show the attribution for each year, and that, for DJF 2024-25, the trend-focused indices (top left panel) were strongly positive and among the strongest amplitudes in the 1991–2025 record. The ENSO-focused index (top right panel) was only weakly negative. The greater amplitude in the trend mode is apparent in the reconstructed patterns (bottom middle panels), which largely reproduced the overall pattern of SST anomalies that was predicted in the tropical oceans by SPEAR (bottom left panels). Trends also mostly accounted for the below-average precipitation predictions extending from California to

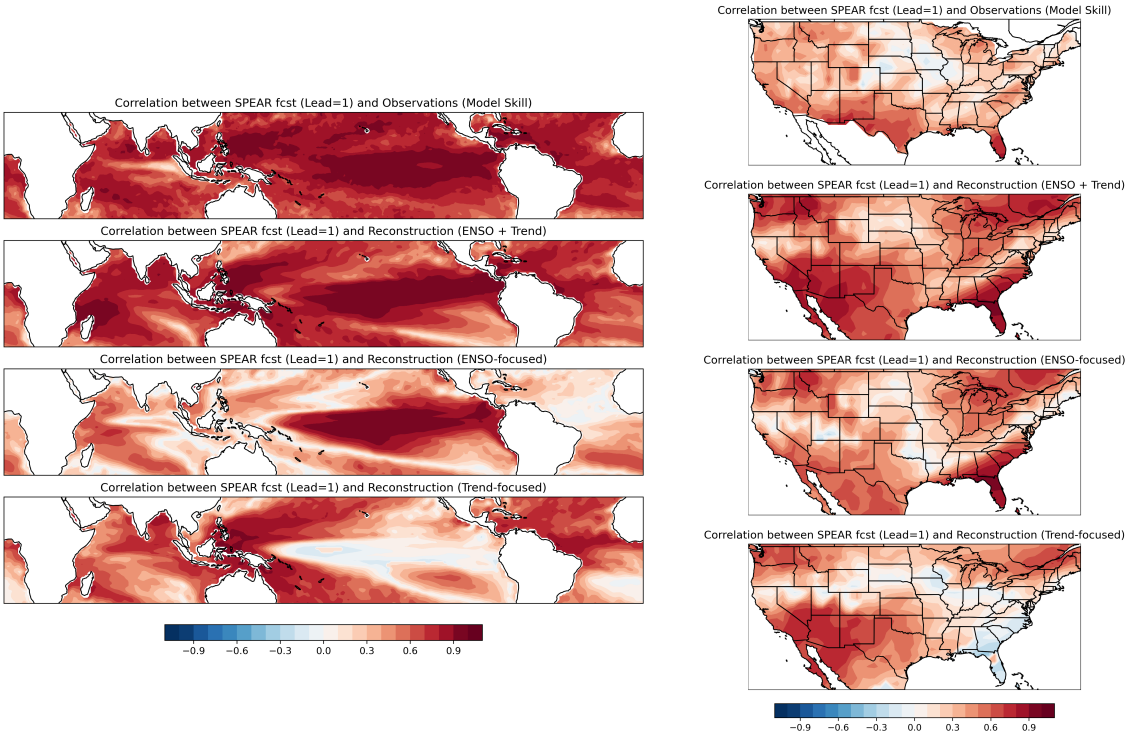

FIG. 10. First lead SPEAR forecast skill from Fig. 6 is reproduced in the top row, alongside SPEAR predictability from ENSO+Trend (second row), ENSO (third row), and Trend (bottom row). To estimate predictability, the reconstructed predictions are correlated against the raw SPEAR forecast. The left panels are based on tropical SST anomalies and the right panels are based on US precipitation anomalies.

Texas and into the lower Mississippi valley. Above average precipitation trends across the northern tier of the U.S. and parts of the southeast were also mirrored in the DJF 2024–25 prediction. While La Niña partially contributed to the intensity of the below-average SSTs in the central and eastern equatorial Pacific and precipitation anomalies over the U.S., they were of much weaker strength. Supp. Fig. 4 shows the summation of the two attribution components next to the prediction and what was observed during DJF 2024–25. There were some differences between the raw model forecasts and observations, which is expected given the observations include both predictable signals and unpredictable noise. Overall, the CCA reconstruction using SPEAR provides a physical interpretation for the model forecast.

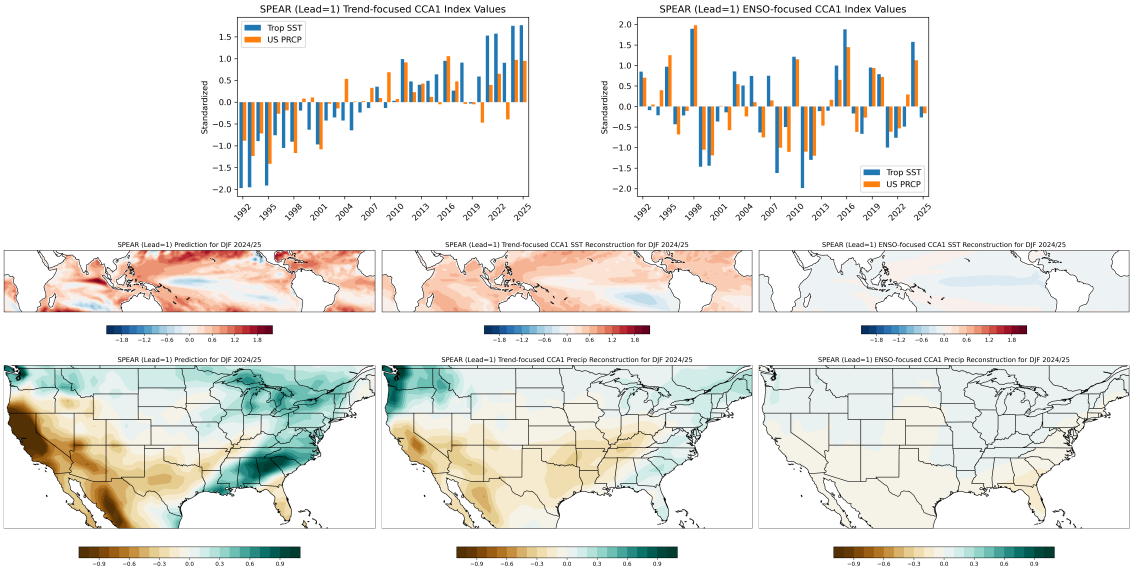

FIG. 11. A forecast attribution focused on the DJF 2024-25 season, using reconstructions based on the Trend-focused and ENSO-focused leading CCA1 shown in Fig. 7. The top row shows the standardized index values from the Trend (left panel) and ENSO-focused (right panel) partial CCA. In the middle and bottom rows, the first lead raw SPEAR prediction for DJF 2024-25 are displayed for tropical SST anomalies and US precipitation anomalies (first column), the reconstructed predictions based on the Trend-focused (middle column) and ENSO-focused (third column) CCA.

5. Summary and Discussion

In this study, CCA is used to diagnose the sources of boreal winter (DJF) predictability in NOAA's most recent state-of-the-art seasonal climate model, the SPEAR. In particular, tropical SST anomalies and contiguous US precipitation anomalies were analyzed to uncover leading patterns of correlated variability. Two CCA modes are able to explain most of the SST and precipitation predictability in SPEAR. Because predictability is prerequisite for skill, these two modes also describe most of the skill as well. Because CCA searches for linear combinations that maximize correlation, the resulting modes are a mix of physically interpretable phenomenon. The top modes are a blend of two different seasonal drivers, ENSO and trends. To separate the predictability sources into physically distinct patterns, partial CCA was used to produce individual modes that represent ENSO variability and linear trends. Reconstructions using these CCA modes reproduce

the prediction skill to the same degree as the original CCA and offer physical interpretability that can be used in forecast attributions.

Additionally, when ENSO and trends are both linearly removed from the data, the remaining CCA modes are weak and statistically insignificant. Further, a reconstruction formed from these residual patterns does not significantly improve winter prediction skill. The resulting decrease in skill, after the removal of ENSO and trends, is a particularly striking result given that CCA is prone to overfit and find correlated patterns with relations that fail to be robust in independent data. Finally, a forecast attribution was provided, with a focus on the 2024–25 winter, showing that the SPEAR predictions of tropical SST and US precipitation were mostly driven by the linear trend, with a borderline La Niña playing a smaller role.

Previously identified tropical SST trend errors in initialized climate models also play a role in SPEAR, with errors trending toward more El Niño-like SST patterns and weaker, less La Niña-like US precipitation anomalies at increasing lead times. While exploring these errors is outside the scope of this study, these trend errors should be considered when providing forecast attributions beyond the shortest leads. Given only a few CCA modes can explain most of the skill in SPEAR, there may be an opportunity to use the observed CCA modes to correct the model predictions at longer forecast leads. However, this strategy would need to be evaluated on historical records beyond the 34-year SPEAR archive to ensure these observed patterns remain robust and are not overly sensitive to sampling.

While splitting correlated variability into trends and no trends is a straightforward decomposition, it excludes the possibility that the ENSO phenomenon itself contains trends. In fact, research argues that coupled processes inherent to ENSO are better isolated by subtracting the tropical SST average (20S-20N) from the Niño-3.4 index (van Oldenborgh et al. 2021; L'Heureux et al. 2024). This newer index is referred to as the "Relative Niño-3.4 index" or "Relative Oceanic Niño Index (RONI)." The relative indices have weak negative trends over the period considered here (1991–2025). Supp. Fig. 5 shows the CCA results if, instead of linearly detrending the SST data, the tropical SST mean is subtracted (precipitation continues to be linearly detrended). The resulting CCA-1 modes are very similar to Fig. 7, except now the "ENSO-focused" CCA1 contains a small negative trend in the time series, which mirrors RONI, and the "Trend-focused" CCA1 has a smaller canonical correlation (r=0.38). However, simply subtracting the tropical mean SST out does not remove

linear trends across the entire tropics (Supp. Fig. 6). These linear trends emerge in successive CCA modes, complicating the physical interpretation by generating multiple trend-like patterns (Supp. Fig. 7). In this study our goal was not to optimize an ENSO index, so we stick to our simpler trend vs. no trend paradigm, but this can be modified depending on one's objectives.

CCA assumes linear relationships, which means there may be physical, non-linear sources of skill that are not emergent in this study. Future work could consider employing methodologies that go beyond linear analysis such as neural networks and deep learning, especially to the model hindcast which offer more samples beyond the limited observational record. However, it is noteworthy that the skill of SPEAR model predictions is captured by the linear CCA patterns. This suggests that while non-linear predictability can exist, either the resulting variability is small enough to be mostly inconsequential for prediction skill or the models are not yet able to represent such non-linear sources of skill.

Acknowledgments. The authors thank two CPC internal reviewers. The scientific results and conclusions, as well as any view or opinions expressed herein, are those of the authors and do not necessarily reflect the views of NWS, NOAA, or the Department of Commerce. MKT acknowledges NOAA Climate Program Office grant NA23OAR4310607.

Data availability statement. SPEAR data are available through the International Research Institute for Climate and Society (IRI) data library at https://iridl.ldeo.columbia.edu/SOURCES/.Models/.NMME/. CPC Unified precipitation and OISSTv2.1 can be accessed through the NOAA/OAR/ESRL/PSL gridded data catalogue https://psl.noaa.gov/data/gridded/index.html.

References

Barnett, T. P., and R. Preisendorfer, 1987: Origins and Levels of Monthly and Seasonal Forecast Skill for United States Surface Air Temperatures Determined by Canonical Correlation Analysis. *Mon. Wea. Rev.*, **115 (9)**, 1825 – 1850, https://doi.org/10.1175/1520-0493(1987)115⟨1825:OALOMA⟩2.0.CO;2.

Barnston, A. G., and C. F. Ropelewski, 1992: Prediction of ENSO Episodes Using Canonical Correlation Analysis. *J. Climate*, **5 (11)**, 1316 – 1345, https://doi.org/10.1175/1520-0442(1992)005⟨1316:POEEUC⟩2.0.CO;2.

Barnston, A. G., and T. M. Smith, 1996: Specification and Prediction of Global Surface Temperature and Precipitation from Global SST Using CCA. *J. Climate*, **9 (11)**, 2660 – 2697, https://doi.org/10.1175/1520-0442(1996)009⟨2660:SAPOGS⟩2.0.CO;2.

Becker, E. J., B. P. Kirtman, M. L'Heureux, A. G. Munoz, and K. Pegion, 2022: A Decade of the North American Multimodel Ensemble (NMME): Research, Application, and Future Directions. *Bull. Amer. Meteor. Soc.*, **103 (3)**, E973 – E995, https://doi.org/10.1175/BAMS-D-20-0327.1.

Beverley, J. D., M. Newman, and A. Hoell, 2024: Climate model trend errors are evident in seasonal forecasts at short leads. *npj Clim. Atmos. Sci.*, **7 (1)**, 285, https://doi.org/10.1038/s41612-024-00832-w.

Bretherton, C. S., C. Smith, and J. M. Wallace, 1992: An Intercomparison of Methods for Finding Coupled Patterns in Climate Data. *J. Climate*, **5 (6)**, 541 – 560, https://doi.org/10.1175/1520-0442(1992)005⟨0541:AIOMFF⟩2.0.CO;2.

Buchmann, P., and T. DelSole, in review: A New Mode of Subseasonal Predictability Over the US: Boreal Summer. *J. Climate*.

Chen, M., A. Kumar, M. L'Heureux, P. Peng, T. Zhang, M. P. Hoerling, and H. F. Diaz, 2024: Why Do DJF 2023/24 Upper-Level 200-hPa Geopotential Height Forecasts Look Different From the Expected El Niño Response? *Geophys. Res. Lett.*, **51 (14)**, e2024GL108 946, https://doi.org/https://doi.org/10.1029/2024GL108946.

Chen, M., W. Shi, P. Xie, V. B. S. Silva, V. E. Kousky, R. Wayne Higgins, and J. E. Janowiak, 2008: Assessing Objective Techniques for Gauge-based analyses of Global Daily Precipitation. *J. Geophys. Res.*, **113 (D4)**, https://doi.org/https://doi.org/10.1029/2007JD009132.

Clark, J. P., N. C. Johnson, M. Park, M. Bernardez, and T. L. Delworth, 2025: Predictable Patterns of Seasonal Atmospheric River Variability Over North America During Winter. *Geophys. Res. Lett.*, **52 (7)**, e2024GL112 411, https://doi.org/https://doi.org/10.1029/2024GL112411.

DelSole, T., and M. Tippett, 2022: *Statistical Methods for Climate Scientists*. Cambridge University Press.

DelSole, T., and M. K. Tippett, 2009a: Average Predictability Time. Part I: Theory. *J. Atmos. Sci.*, **66 (5)**, 1172–1187, https://doi.org/10.1175/2008JAS2868.1.

DelSole, T., and M. K. Tippett, 2009b: Average Predictability Time. Part II: Seamless Diagnoses of Predictability on Multiple Time Scales. *J. Atmos. Sci.*, **66 (5)**, 1188 – 1204, https://doi.org/10.1175/2008JAS2869.1.

DelSole, T., and M. K. Tippett, 2021: A mutual information criterion with applications to canonical correlation analysis and graphical models. *Stat*, **10 (1)**, e385, https://doi.org/https://doi.org/10.1002/sta4.385.

Delworth, T. L., and Coauthors, 2020: SPEAR: The Next Generation GFDL Modeling System for Seasonal to Multidecadal Prediction and Projection. *J. Adv. Model. Earth Syst.*, **12 (3)**, e2019MS001 895, https://doi.org/https://doi.org/10.1029/2019MS001895.

Hotelling, H., 1936: Relations Between Two Sets of Variates. *Biometrika*, **28 (3-4)**, 321–377, https://doi.org/10.1093/biomet/28.3-4.321.

Huang, B., C. Liu, V. Banzon, E. Freeman, G. Graham, B. Hankins, T. Smith, and H.-M. Zhang, 2021: Improvements of the Daily Optimum Interpolation Sea Surface Temperature (DOISST) Version 2.1. *J. Climate*, **34 (8)**, 2923 – 2939, https://doi.org/10.1175/JCLI-D-20-0166.1.

Jia, L., T. L. Delworth, X. Yang, W. Cooke, N. C. Johnson, C. McHugh, and F. Lu, 2023: Seasonal prediction of North American wintertime cold extremes in the GFDL SPEAR forecast system. *Climate Dyn.*, **61 (3)**, 1769–1781, https://doi.org/10.1007/s00382-022-06655-w.

Kirtman, B. P., and Coauthors, 2014: The North American Multimodel Ensemble: Phase-1 Seasonal-to-Interannual Prediction; Phase-2 toward Developing Intraseasonal Prediction. *Bull. Amer. Meteor. Soc.*, **95 (4)**, 585 – 601, https://doi.org/10.1175/BAMS-D-12-00050.1.

L'Heureux, M. L., M. K. Tippett, and W. Wang, 2022: Prediction Challenges From Errors in Tropical Pacific Sea Surface Temperature Trends. *Frontiers in Climate*, **Volume 4 - 2022**, https://doi.org/10.3389/fclim.2022.837483.

L'Heureux, M. L., and Coauthors, 2024: A Relative Sea Surface Temperature Index for Classifying ENSO Events in a Changing Climate. *J. Climate*, **37 (4)**, 1197 – 1211, https://doi.org/10.1175/JCLI-D-23-0406.1.

Mayer, M., M. A. Balmaseda, F. Vitart, and S. Tietsche, 2025: Tropical Pacific Trends in the ECMWF Seasonal System and Implications for Predictions of the 2020–22 Triple-Dip La Niña. *J. Climate*, **38 (13)**, 2989 – 3003, https://doi.org/10.1175/JCLI-D-24-0467.1.

Mo, K. C., 2003: Ensemble Canonical Correlation Prediction of Surface Temperature over the United States. *J. Climate*, **16 (11)**, 1665 – 1683, https://doi.org/10.1175/1520-0442(2003)016⟨1665:ECCPOS⟩2.0.CO;2.

Mo, K. C., and W. M. Thiaw, 2002: Ensemble canonical correlation prediction of precipitation over the Sahel. *Geophys. Res. Lett.*, **29 (12)**, 11–1–11–4, https://doi.org/https://doi.org/10.1029/2002GL015075.

Patterson, M., D. J. Befort, J. F. Lockwood, J. Slattery, and A. Weisheimer, 2025: The Representation of Surface Temperature Trends in C3S Seasonal Forecast Systems. *Atmos. Sci. Lett.*, **26 (8)**, e1316, https://doi.org/https://doi.org/10.1002/asl.1316.

Pegion, K., E. Becker, and B. P. Kirtman, 2026: Sources of Subseasonal Predictability for Precipitation in South America Based on Model Experiments. *J. Geophys. Res.*, **131 (4)**, e2025JD044 428, https://doi.org/https://doi.org/10.1029/2025JD044428.

Rana, S., J. Renwick, J. McGregor, and A. Singh, 2018: Seasonal Prediction of Winter Precipitation Anomalies over Central Southwest Asia: A Canonical Correlation Analysis Approach. *J. Climate*, **31 (2)**, 727 – 741, https://doi.org/10.1175/JCLI-D-17-0131.1.

Riddle, E. E., A. H. Butler, J. C. Furtado, J. L. Cohen, and A. Kumar, 2013: CFSv2 ensemble prediction of the wintertime Arctic Oscillation. *Climate Dyn.*, **41 (3)**, 1099–1116, https://doi.org/10.1007/s00382-013-1850-5.

Shin, C.-S., and B. Huang, 2019: A spurious warming trend in the NMME equatorial Pacific SST hindcasts. *Climate Dyn.*, **53 (12)**, 7287–7303, https://doi.org/10.1007/s00382-017-3777-8.

Tippett, M. K., and E. J. Becker, 2024: Trends, Skill, and Sources of Skill in Initialized Climate Forecasts of Global Mean Temperature. *Geophys. Res. Lett.*, **51 (16)**, e2024GL110 703, https://doi.org/https://doi.org/10.1029/2024GL110703.

Tippett, M. K., T. DelSole, S. J. Mason, and A. G. Barnston, 2008: Regression-Based Methods for Finding Coupled Patterns. *J. Climate*, **21 (17)**, 4384 – 4398, https://doi.org/10.1175/2008JCLI2150.1.

van Oldenborgh, G. J., H. Hendon, T. Stockdale, M. L'Heureux, E. Coughlan de Perez, R. Singh, and M. van Aalst, 2021: Defining El Niño indices in a warming climate. *Environ. Res. Lett.*, **16 (4)**, 044 003, https://doi.org/10.1088/1748-9326/abe9ed.

Wallace, J. M., C. Smith, and C. S. Bretherton, 1992: Singular Value Decomposition of Wintertime Sea Surface Temperature and 500-mb Height Anomalies. *J. Climate*, **5 (6)**, 561 – 576, https://doi.org/10.1175/1520-0442(1992)005⟨0561:SVDOWS⟩2.0.CO;2.

Wang, G., Y. Zhuang, R. Fu, S. Zhao, and H. Wang, 2021: Improving Seasonal Prediction of California Winter Precipitation Using Canonical Correlation Analysis. *J. Geophys. Res.*, **126 (17)**, e2021JD034 848, https://doi.org/https://doi.org/10.1029/2021JD034848.

Zhang, W., B. Xiang, K.-C. Tseng, N. C. Johnson, L. Harris, T. Delworth, and B. Kirtman, 2024: Subseasonal-to-seasonal (S2S) prediction of atmospheric rivers in the Northern Winter. *npj Clim. Atmos. Sci.*, **7 (1)**, 275, https://doi.org/10.1038/s41612-024-00827-7.

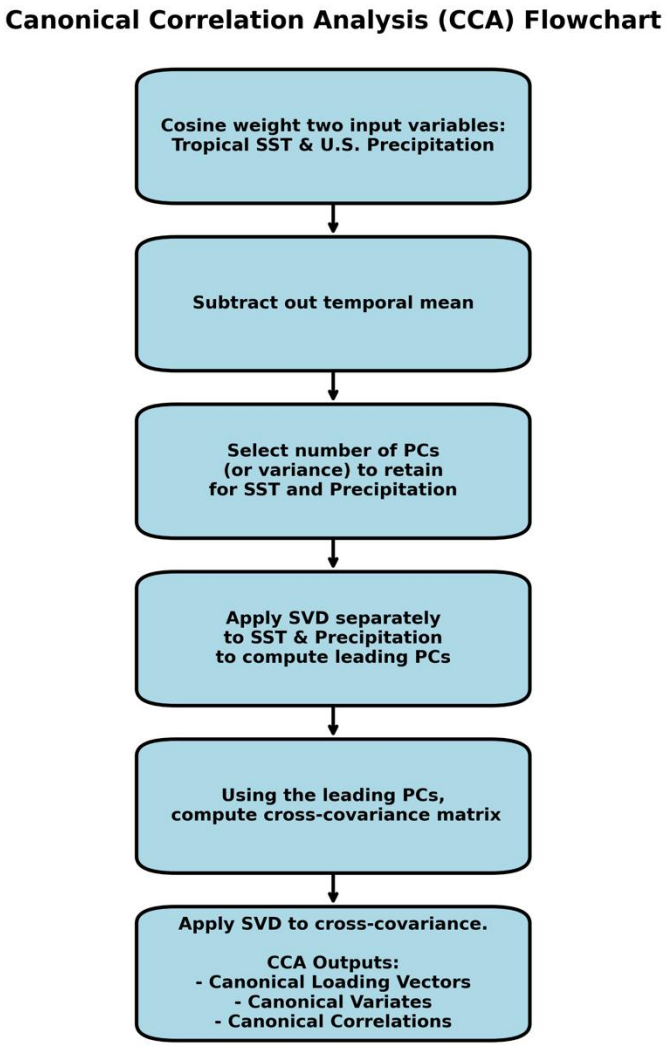

Supp. Figure 1: Steps to calculate Canonical Correlation Analysis (CCA).

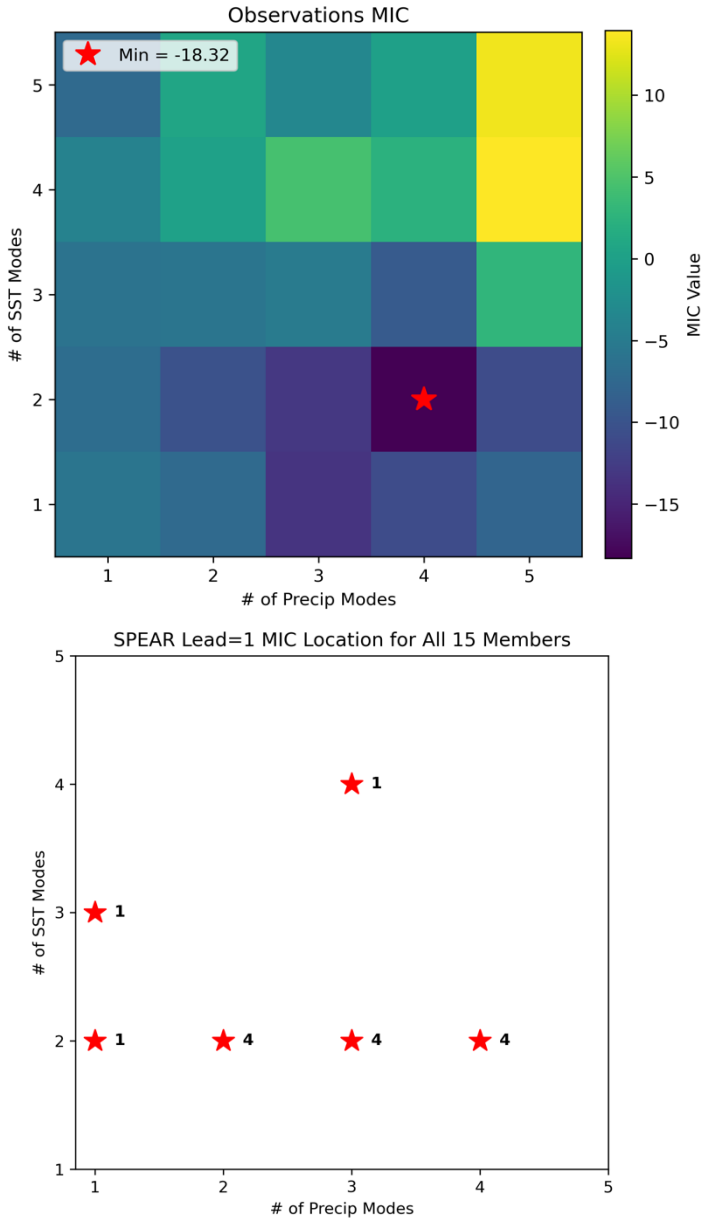

Supp. Figure 2: Mutual Information Criterion (MIC), with red stars indicating the location of the minimum MIC value and optimal principal component (PC) truncation. Top panel is the MIC based on observations and bottom panel shows the MIC based on all 15 members of SPEAR (Lead=1). Numbers indicate how many members had a minimum MIC at a particular PC combination.

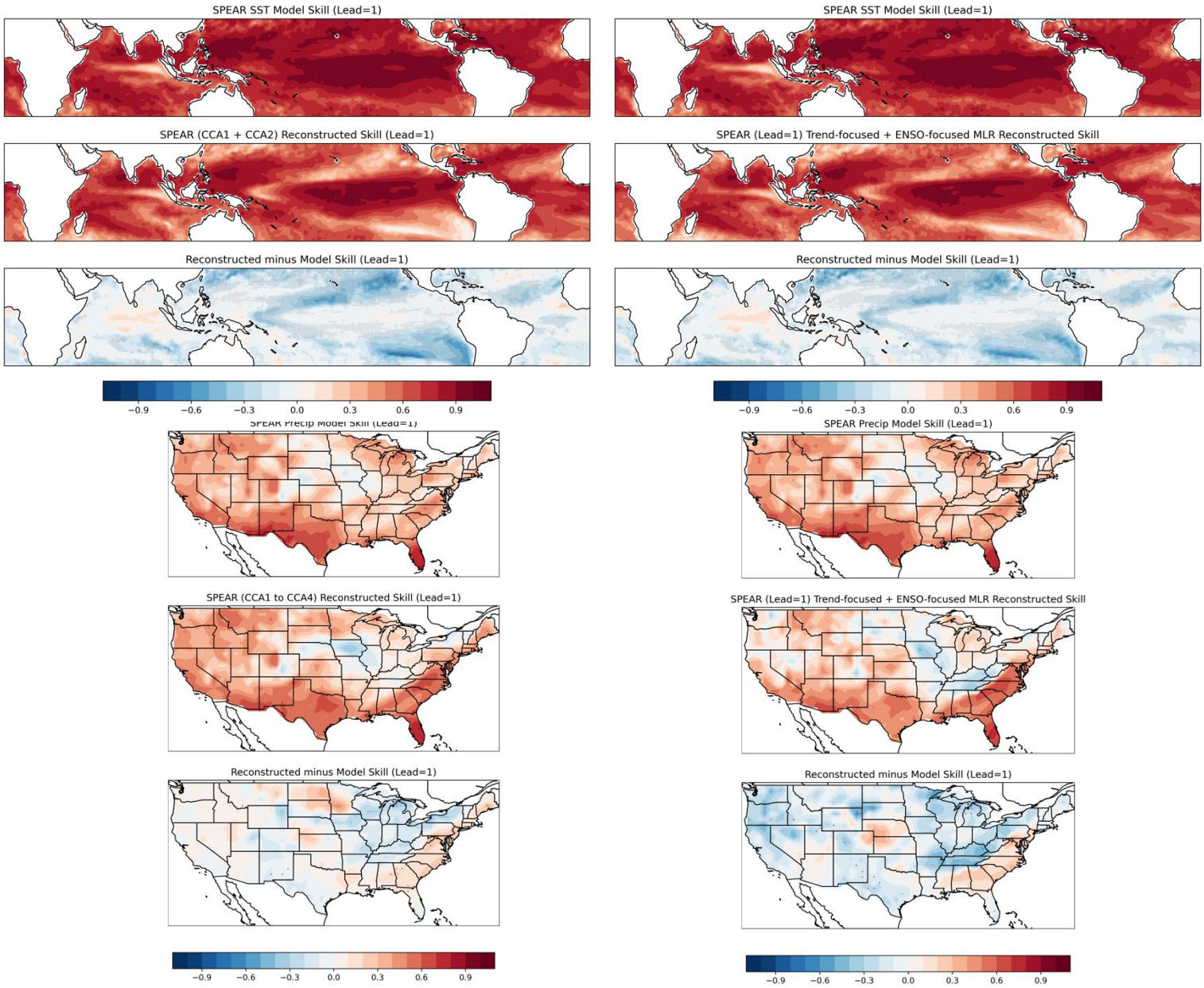

Supp. Figure 3: Figure 6 is reproduced in the left column. Multiple linear regression (MLR) is used to combine the leading ENSO-focused and Trend-focused CCA time series, with the skill of the MLR reconstruction displayed in the second and fifth rows of the right column. The difference between the skill of the reconstruction and the SPEAR prediction (first and fourth rows) is presented in the third and sixth rows.

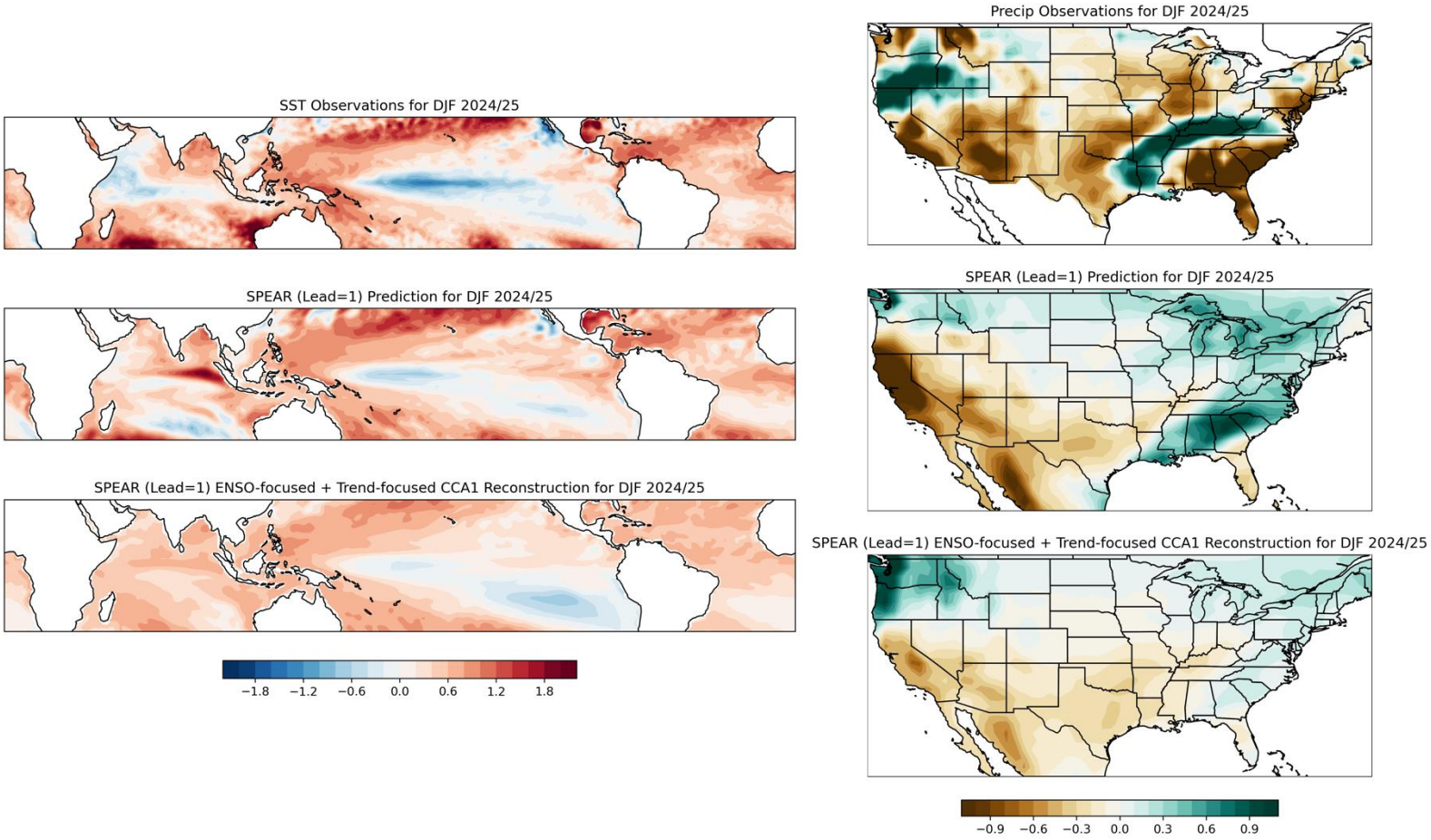

Supp. Figure 4: Observed SST anomalies (left) and U.S. precipitation anomalies (right) for December-February 2024-25 (top row), the first-lead SPEAR prediction (middle row), and the summation of the leading ENSO-focused and Trend-focused reconstructions (bottom row).

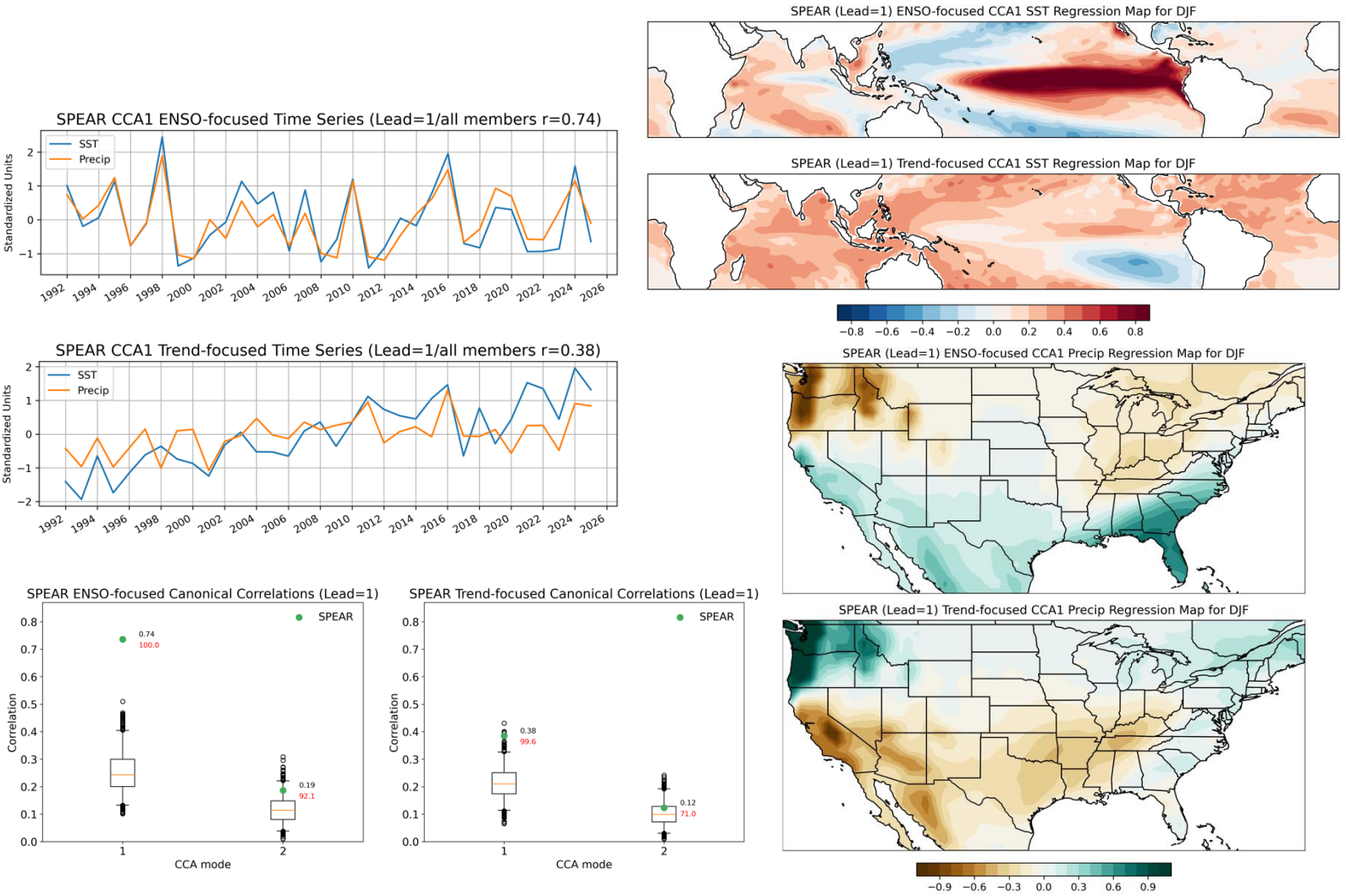

Supp. Figure 5: As in Figure 7, except showing the leading ENSO-focused and Trend-focused CCA modes after the tropical mean (20˚S-20˚N) is subtracted from the SST anomalies. U.S. precipitation is linearly detrended.

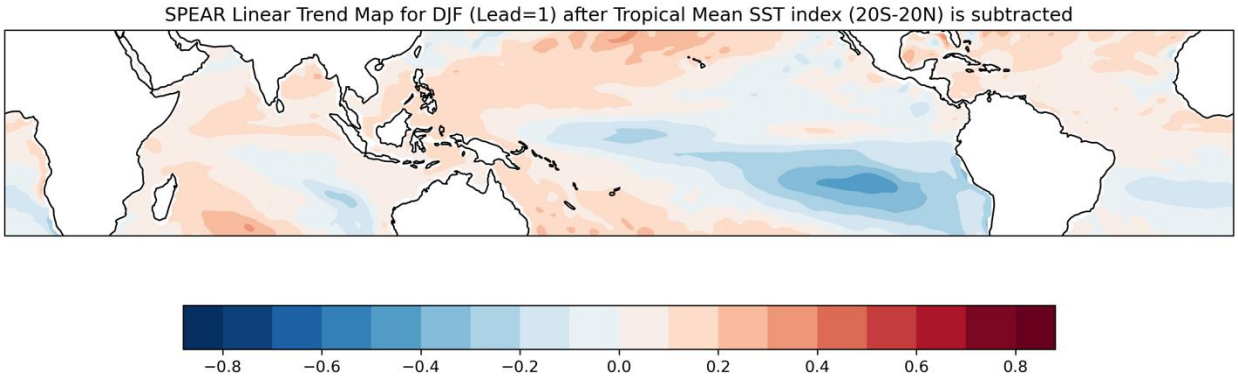

Supp. Figure 6: As in Figure 3, except showing first-lead SPEAR linear trends in SST anomalies after the tropical mean (20˚S-20˚N) is subtracted from the SST anomalies.

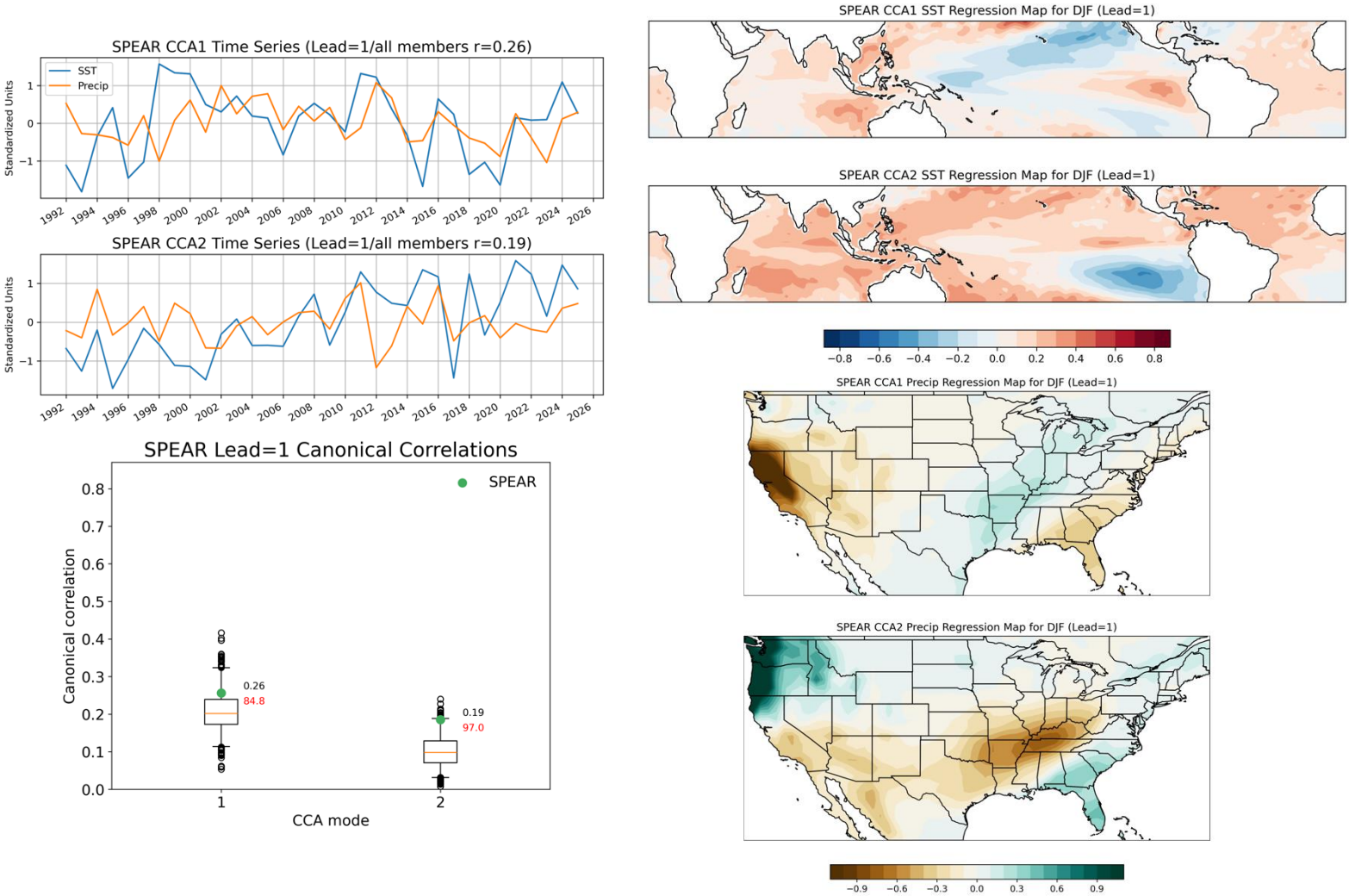

Supp. Figure 7: As in Figure 8, except showing the leading two CCA patterns after the tropical mean (20˚S-20˚N) is subtracted from the SST anomalies (U.S. precipitation is linearly detrended) and the relative Niño-3.4 index is linearly removed.